Canonical profiles and transport model for the toroidal rotation in tokamaks

Yu.N. Dnestrovskij 1), V.F. Andreev 1), A.V. Danilov 1), A.Yu. Dnestrovskij 1), S.V. Cherkasov 1), S.E. Lysenko 1), T.C. Hender 2), C.M. Roach 2), I.A. Voitsekhovich 2), JET EFDA and MAST contributors

1) RRC 'Kurchatov Institute', Tokamak Physics Institute, Moscow, Russia
2) EURATOM/CCFE Fusion Association, Culham Science Centre, Abingdon, Oxon, OX14 3DB, UK

E-mail contact of main author: dnyn@nfi.kiae.ru

Abstract. The equilibrium equation for a rotating plasma is constructed supposing the thermal Mach number is much less than unity. The canonical profile of angular rotation velocity is defined as the profile which minimizes the total plasma energy while conserving toroidal current and obeying the equilibrium condition. The transport model based on this canonical profile, with stiffness calibrated by JET data, reasonably describes the velocity of the forced toroidal rotation. The RMS deviations of the calculated rotation profiles from the experimental ones do not exceed 10-15%. The developed model is also applied to the modeling of MAST rotation.

1. Introduction

Toroidal rotation of plasma occurs in all tokamaks. In accordance with torque mechanism it can be divided for middle size tokamaks into two types:
1) intrinsic rotation, for which the rotation velocity v_t is usually limited in experiment by the condition:

$$v_t < (2\text{-}4) \times 10^6 \text{ cm/s} = 20 - 40 \text{ km/s} \qquad (1)$$

2) forced rotation with rather large velocities

$$v_t < (2\text{-}4) \times 10^7 \text{ cm/s} = 200 - 400 \text{ km/s} \qquad (2)$$

The level of forced rotation is determined by the input of external angular momentum (torque) T. The most widespread source of torque now is neutral beam injection [1-2]. In this report we discuss forced rotation only.

2. The equilibrium equation for rotating plasma

The velocity of toroidal rotation is as follows: $v_t = v_t(\psi, R) = \omega R$, where $\omega = \omega(\psi)$ is an angular frequency, R is the distance from the major axis of torus, ψ is the poloidal magnetic flux. The equilibrium equation for rotating plasma can be written as

$$\Delta^*\psi = - R j_\varphi = - (FF' + R^2 p') \qquad p = p(\psi, R) \qquad (3)$$

where p is a plasma pressure, F is the toroidal field function $F=RB_t$. In sections 2 and 3 the prime designates the derivative with respect to ψ. The dependence on R has to satisfy the condition

$$\partial p/\partial R = \rho_m v_t^2 / R = \rho_m R \omega^2. \qquad (4)$$

Here ρ_m is the mass density of plasma ($\rho_m = n\, m_i$, n is the plasma density, m_i is the ion mass). We suppose that the kinetic energy of plasma rotation is much less than the thermal energy

$$\rho_m v_t^2/2 << p, \quad \text{or} \qquad v_t^2 << v_T^2 \qquad (M^2 = v_t^2/ v_T^2 << 1). \qquad (5)$$

Here v_T is the ion thermal velocity, $M = v_t/v_T$ is the thermal Mach number. We choose the simplest form of the function $p(\psi, R)$, which satisfies the condition (4) as:

$$p = p_0(\psi) + R^2/R_0^2\, p_1 \tag{6}$$

where $p_0(\psi)$ is the usual thermal pressure for non rotating plasma

$$p_1 = (R_0^2/2)\, \rho_m \omega^2 \tag{7}$$

and R_0 is a major radius of plasma. From relation (5)

$$p_1 << p_0, \tag{8}$$

so in the expression for p_1 (7) we can accept that ρ_m and p_1 are independent on R. Therefore $n = n(\psi)$ and $p_1 = p_1(\psi)$. As a result, the equilibrium equation (3) has the form

$$\Delta^*\psi = - R\, j_\varphi = - \{FF' + R^2\, (p_0' + R^2/R_0^2\, p_1')\} \tag{9}$$

Now we consider the variation problem. The canonical profiles of pressure, rotation and poloidal current can be defined as those minimizing the total plasma energy while conserving the toroidal current and satisfying equation (9). The total plasma energy W and the toroidal current I_p are

$$W = \int_V dV\ \{[F^2 + (\nabla\psi)^2]/(2R^2) + 3/2\ p + \rho_m v_t^2/2\}, \quad I_p = 1/(2\pi R) \int_V dV\ (FF' + R^2 p')/R \tag{10}$$

The generalized Lagrange functional has the form:

$$\Phi = W - 2\pi\lambda\ I_p \tag{11}$$

Its first variation in the extreme point should be equal to zero

$$\delta\Phi = \int_V dV\ \delta\psi\ \{[(FF' - \Delta^*\psi)/R^2 + 3/2\ (p_0 + R^2/R_0^2\, p_1)'] -$$
$$- \lambda[(F'F' + FF'')/R^2 + (p_0 + R^2/R_0^2\, p_1)'']\} = 0 \tag{12}$$

From this and (9) we obtain the 2D Euler equation

$$[2FF'/R^2 - \lambda[(FF')'/R^2] + (5/2\ p_0' - \lambda p_0'') + R^2/R_0^2\ [5/2\ p_1' - \lambda p_1''] = 0 \tag{13}$$

The second term in (13) is constant over the magnetic surface, but other terms are not. From this we obtain three independent 1D equations

$$2FF' - \lambda(FF')' = 0, \qquad 5/2\ p_0' - \lambda\ p_0'' = 0, \qquad 5/2\ p_1' - \lambda\ p_1'' = 0 \tag{14}$$

Here first and second equations coincide with corresponding equations for a stationary plasma [3]. The third equation for p_1 coincides with the equation for p_0. Thus, the canonical profile for the function $p_1 = (R_0^2/2)\, \rho_m \omega^2$ coincides with the canonical profile for the function p_0.
The solutions of equations (14) are the functions

$$FF' = C_F \exp(\psi/\lambda), \quad p_0' = C_p \exp(5\psi/4\lambda), \qquad p_1' = C_{p1} \exp(5\psi/4\lambda) \tag{15}$$

Substituting (15) to (9), we obtain the equation for the canonical equilibrium:

$$\Delta^*\psi = - R\, j_\varphi = - \{C_F \exp(\psi/\lambda) + C_p\, R^2 \exp(5\psi/4\lambda)\ (p_0(0) + R^2 \rho_{m0}\, \omega_0^2/2)\} \tag{16}$$

Here we define that on the magnetic axis $\psi = 0$, $\rho_{m0} = \rho_m(0)$, $\omega_0 = \omega(0)$. The parameters C_F, C_p and λ have to be defined from additional conditions, for example:

$$\psi\,|_S = \psi_a, \qquad q(0) = q_0 \qquad I_p \text{ is prescribed} \tag{17}$$

In the case of a circular cylinder Eq. (16) has the form:

$$- \Delta\psi = C_F \exp(\psi/\lambda) + C_p \exp(5\psi/4\lambda) \quad (18)$$

If we put $C_p = 0$ (low plasma pressure), we obtain

$$1/r \, d/dr \, (r \, d\psi/dr) = \psi'' + \psi'/r = - C_F \exp(\psi/\lambda) \quad (19)$$

The solution of this equation has the form:

$$\psi/\lambda = - \ln(1+Dr^2)^2 \quad (20)$$

Substituting (20) into (19), we find the link between parameters D, λ and C_F. Then it is straightforward to find the poloidal magnetic field B_θ, $\mu = 1/q$ and the current density j:

$$B_\theta = C_F/2 \, [r/(1+Dr^2)], \quad \mu = R \, B_\theta/(rB_0) = \mu_0/(1+Dr^2), \quad j = j_0/(1+Dr^2)^2 \quad (21)$$

The constant D is defined by boundary conditions. Expressions (21) coincide with Kadomtsev's formulae based on the minimization of the poloidal magnetic energy functional [4]. This coincidence is a basis for conclusions given in the following section.

3. Canonical profile for angular rotation frequency

Taking into account that the canonical profiles are defined with accuracy of multiplier and using the result from previous section that $p_{c1} \propto p_{c0}$, we obtain

$$p_{c1} \propto p_{c0} \propto \rho_{mc} \, \omega_c^2 \propto n_c \, \omega_c^2 \propto n_c \, T_c \quad (22)$$

therefore

$$T_c \propto \omega_c^2 \quad (23)$$

The canonical profiles here are denoted by the subscript "c". The canonical profile for temperature was defined in our previous papers [5, 6]. In particular there was shown that $T_c \propto p_c^{2/3}$. From this we obtain

$$\omega_c \propto T_c^{1/2} \propto p_{0c}^{1/3} \quad (24)$$

In the transport model we will use the logarithmic derivatives of different variables. From (24), they are linked by following relations

$$\omega_c'/\omega_c = 1/3 \, p_{0c}'/ p_{0c} \quad = ½ \, T_c'/ T_c \quad (25)$$

Here and below the prime now denotes the derivative over the dimensional radial coordinate ρ, which defines the magnetic surface ($0 < \rho < \rho_{max}$). The canonical profiles for the current and pressure were defined in [5, 6].

4. Transport model of canonical profiles

4.1. Linear model for toroidal rotation

The specific angular momentum is defined as:

$$L_0 = n \, m_i \, R \, v_t = n \, m_i \, R^2 \, \omega \quad (26)$$

We assume that the radial flux of the angular momentum q_ω is proportional to the difference between the relative gradient of calculated momentum and the relative gradient of canonical momentum (similarly to the heat and particle fluxes). In the linear model this flux is equal to

$$q_\omega = - n \, m_i \, R^2 \, \chi_\omega^{PC} \, \omega \, (\omega'/\omega - \omega_c'/\omega_c) \quad (27)$$

The equation for momentum has the form

$$\partial/\partial t \, L_0 = - \mathrm{div}_\rho \, (q_\omega) + n \, \Phi \, R \quad (28)$$

where Φ is the force applied to a mass corresponding to 1 m^3. After integration of (28) over the plasma volume, we obtain

$$\partial L/\partial t = - L/\tau_\omega + T \qquad (29)$$

where

$$L = \int_V dV\, L_0, \qquad T = \int_V dV\, n\Phi R \qquad (30)$$

are the total angular momentum and total torque, $L/\tau_\omega = - q_{\omega a}$, τ_ω is the angular momentum confinement time: $\tau_\omega = L / (T - \partial L/\partial t)$. In the steady state

$$\tau_\omega = L /T \qquad (31)$$

Usually in the experiment τ_ω is close to the energy confinement time τ_E.

4.2. Nonlinear model for the electron and ion temperatures and plasma density

This model was published in [7, 8]. The heat and particle fluxes, q_α (α = e, i), Γ, are described by the following expressions:

$$q_\alpha = - n\chi_\alpha^{PC} T_\alpha (T_\alpha'/T_\alpha - T_c'/T_c)\, H(-[T_\alpha'/T_\alpha - T_c'/T_c])\, F_\alpha - n\chi_\alpha^{0}\, T_\alpha' + 3/2\, \Gamma T_\alpha \qquad (32)$$

$$\Gamma = - D\, n\, (p_e'/p_e - p_c'/p_c)\, F_e\, F_i - D^0\, n' + \Gamma^{neo}, \qquad (33)$$

where T_α and n are the temperatures and density to be determined, T_c and p_c are the canonical profiles of temperature and pressure, χ_α^{PC} and D are stiffness coefficients, $\Gamma^{neo} = n\, \nu^{neo}$, $H(x)$ is the Heaviside function, ρ is a radial coordinate ($0 < \rho < \rho_{max}$). The values of χ_α^{PC} were found earlier by the comparison of calculations with experiment [9, 6]:

$$\chi_\alpha^{PC} = C_{T\alpha}\, (1/M)\, (a/R)^{0.75} q(\rho = \rho_{max}/2) q_{cyl}\, (T_e(\rho = \rho_{max}/4))^{1/2}\, (3/R)^{1/4}\, (1/B_0)\, \bar{n}/n \qquad (34)$$

where a and R are minor and major radii, B_0 is the toroidal magnetic field, M is ion mass number, $q_{cyl}=B_0 a^2/2I_p R$, I_p is the plasma current. We use everywhere n, I_p, P_{tot}, R, $T_{e,i}$ and χ in $10^{19} m^{-3}$, MA, MW, m, keV, m^2/s respectively, <…> denotes volume-averaging, P_{tot} is the auxiliary power deposited into plasma. We also set [10, 7] $D = C_n \chi_e^{PC}$, $C_n = 0.08$, χ_i^0 (m^2/s) = $0.07\, P_{tot}/ I_p$, $\chi_e^0 = \chi_i^0\, \{2.25\, (T_e)^{1/2}/R\}$, $D^0 = 0.26\, (T_e(0))^{1/2}/(<n>R)$.

The values of χ_α^0 and D^0 are much smaller than χ_α^{PC} and D, but they play an essential role inside the transport barriers. We use also the following boundary condition for canonical profile [10]: $\mu_c(0) = (3.5 – 4)\, \mu_c(a)$, where the value of $\mu_c(a)$ is defined by the solution of the equilibrium Grad-Shafranov equation.

To describe the barrier formation we use the possibility of bifurcation due to nonlinearities in transport equations [11]. Such a nonlinearity is included in (32)-(33) using the function F_α as follows:

$$F_\alpha = \exp(-z_{p\alpha}^2/2z_0^2), \qquad (35)$$

where $z_{p\alpha} = -(a\, \rho_{max}/\rho)\, (p_\alpha'/p_\alpha - p_c'/p_c)$ is a dimensionless “distance” between the electron or ion pressure profiles and the canonical pressure profile. The form of F_α means that the transport barrier occurs, when the distance $z_{p\alpha}$ exceeds the critical gradient z_0: $|z_{p\alpha}| > z_0$. Note that inside the transport barrier $F_k << 1$ and the first terms in fluxes (32)-(33) will be small, but outside this region $F_k \approx 1$. In the transient regime the parameter z_0 determines the L-H transition threshold, but at the steady-state it determines the width of transport barrier. The range of z_0 for different devices was explored in [11]: z_0 = 6-9. A more precise estimate of z_0

is only essential for the determination of the threshold power of the L-H transition. A rough estimate of z_0 is sufficient to describe the developed H-mode. Here we put $z_0 = 8$. With this choice the ETB width, which arises as a result of bifurcation, usually equals to 3-5% of minor plasma radius - this value does not contradict experiment. Note that the transport model described in (32)-(35) does not include the effects of rotation on the transport properties of plasma. Such effects were discovered many years ago in experiment and were described recently in [12, 13].

4.3. Transport coefficient for the linear model of rotating plasma

We assume that the stiffness of the angular frequency profile χ_ω^{PC} is proportional to the stiffness of the electron temperature profile:

$$\chi_\omega^{PC} = C_\omega \chi_e^{PC}, \qquad (36)$$

where χ_e^{PC} is defined by (34). We determined C_ω using 11 JET shots from the International Multi-tokamak Confinement Profile database [14] (Table 1). The transport equations were solved in the interval ($0 < \rho < \rho_{max}$). Boundary conditions at the point $\rho = \rho_{max}$ are taken from the experiment: $\omega(\rho_{max}) = 8 – 22$ (krad/s). Due to errors in experimental values of $\omega(\rho_{max})$, we have chosen $\omega(\rho_{max})$ to optimise the solution of the equation for ω to fit the experimental values of ω_{exp} in the zone $\rho/\rho_{max} \sim 0.8$ - 0.9. For each shot we optimise C_ω to give the best fit to experimental measurements during the steady-state phase of discharge. The results of calculations may be approximated by formula:

$$C_\omega = 1/n^{1/3} \qquad (n \text{ in } 10^{19}\,\text{m}^{-3}) \qquad (37)$$

We see that at high densities the rotation stiffness is rather less than the electron temperature stiffness. We will assess the accuracy of the simulation using the RMS deviations between calculated and measured profiles. The temperature deviation may be written as:

$$d_2T = \{(1/N) \sum_{k=1}^{N} [\frac{T_k^{calc} - T_k^{exp}}{T_k^{exp}}]^2 \}^{1/2} \qquad (38)$$

Similar formulae are used for density and angular frequency. Although the experimental data obtained by TRANSP are finite over the whole plasma cross section, there are really no measurements of the velocity at $\rho > 0.8\ \rho_{max}$. Therefore we only sum in (38) over the region ($0 < \rho < 0.8\ \rho_{max}$).

5. Results of calculations

The calculated and experimental profiles of angular rotation frequency, $\omega(\rho)$ and $\omega_{exp}(\rho)$, at t = 11 s for hybrid H-mode shot #60933 are shown in Fig. 1. We see their reasonable agreement. Figure 2 presents the temporal evolution of four deviations: d_2T_e, d_2T_i, d_2n and $d_2\omega$ for the same shot. The first three deviations are calculated with the nonlinear model presented in section 4.2; the fourth deviation is obtained by the calculations with the linear model presented in section 4.1. The next figures illustrate the shot #52009 with the H-mode and rather high density. Figure 3 shows the temporal evolution of the total input NBI power P_{NBI}, line-averaged density $\bar{n}$, and experimental and calculated central electron temperatures, T_{ex0}, T_{e0}. We see that the quasi- steady state phase in this shot lasts at least 6 s (17 s < t< 23 s).

TABLE 1. Parameters of studied shots.

#	Shot #	Current	Power	Density	Torque	Comment
		I_p, MA	P_{NBI}, MW	n, 10^{19} m^{-3}	T, N m	
1	38285	2.5	12	6	11	H-mode
2	38287	2.5	12	5	10	H-mode
3	52009	2.5	15	7.5	14	H-mode
4	52014	2.5	13.5	10.5	10	H-mode
5	52015	2.5	13.5	10	12	H-mode
6	52022	2.5	15	9	11.5	H-mode
7	52024	2.5	15	10	11.5	H-mode
8	52025	2.5	15	8.5	12.5	H-mode
9	60927	1.4	13	3.5	13	Hybrid
10	60931	1.4	17	3.5	17	Hybrid
11	60933	2.0	15.5	3	22	Hybrid

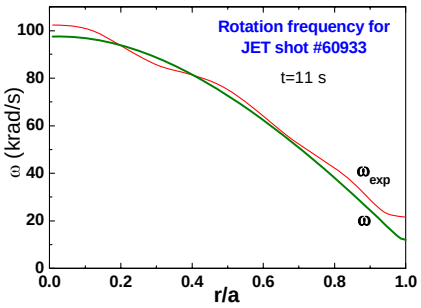

FIG. 1.Calculated and experimental rotation frequencies for low-density JET shot.

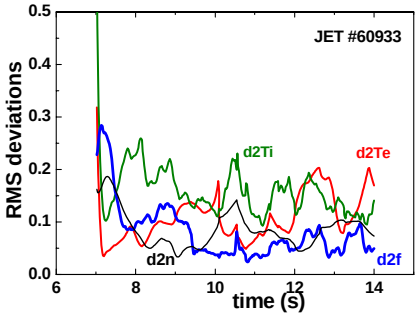

FIG. 2. The temporal evolution of temperature, density and rotational frequency deviations of calculations from experiment for the same shot.

Figure 4 shows the temporal evolution of the deviations of electron temperature, density and angular frequency in the same shot. During the rapid density ramp-up, the simulation procedure adjusts the calculated density with some delay, so the RMS density deviation d_2n is as large as 20%, and the deviations of temperature and frequency are also at the level of 20-25%. However, in the second part of steady state phase, for 20 s< t < 23 s, the calculated density is reasonable (d_2n ~ 3-5%) and the temperature and frequency deviations decrease to the level of 5-10%. The next figure presents the data for shot #52014, a very high density H-mode plasma. Such a high density leads to peripheral deposition of beam particles, which transfer their torque to plasma ions also at the periphery (Fig. 5). However, the experimental profile of angular frequency has maximum at the plasma center. Such plasma behaviour may be evidence of an anomalous momentum pinch, directed to the plasma center. This momentum pinch is intrinsic in our model, when the first term in brackets for the momentum flux in (27) is less than the second one. Such an anomalous torque pinch was seen in experiment also [15].

Figure 6 presents the momentum confinement time τ_ω (a) (Eq. (31)) and the ratio τ_ω/τ_E (b) as functions of the plasma density for shots with rather high plasma currents (I_p>1.5 MA) at the quasi steady-state phase of discharges. At high densities the profiles of input power are hollow, and the energy rapidly escapes from plasma. However, owing to the strong pinch of angular momentum (illustrated by Fig. 5) the momentum confinement time increases during the density ramp-up. The ratio τ_ω/τ_E grows from small values (~ 0.5) at low densities up to values exceeding unity (~ 2) at high densities.

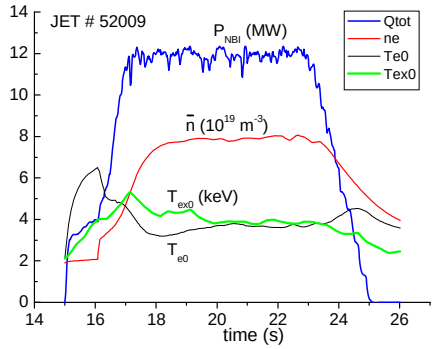

FIG. 3. Temporal evolution of the NBI power P_{NBI}, line-averaged density $\bar{n}$, and experimental and calculated central electron temperatures, T_{ex0}, T_{e0} for the JET shot #52009 with the H-mode and rather high density

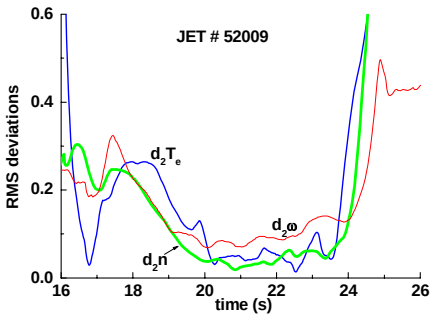

FIG. 4. Deviations of the calculated electron temperature, density and angular frequency from experimental ones for the same JET shot.

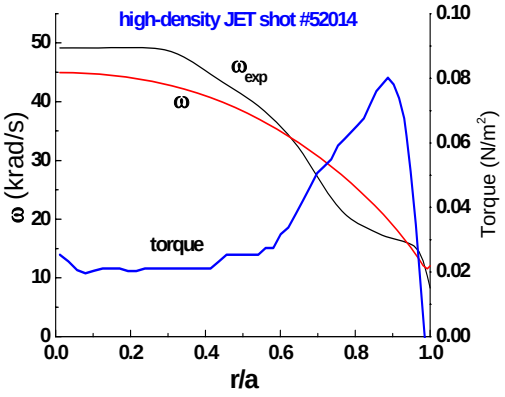

FIG. 5. Profiles of experimental ω_{exp} and calculated angular frequency ω, and input specific torque for high-density JET shot #52014 at t = 21 s.

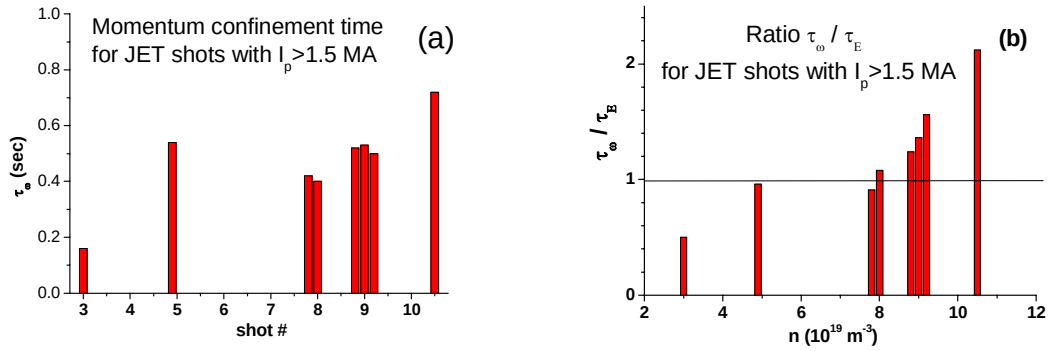

FIG. 6. The momentum confinement time τ_ω (a) and the ratio τ_ω/τ_E (b) as functions of the plasma density.

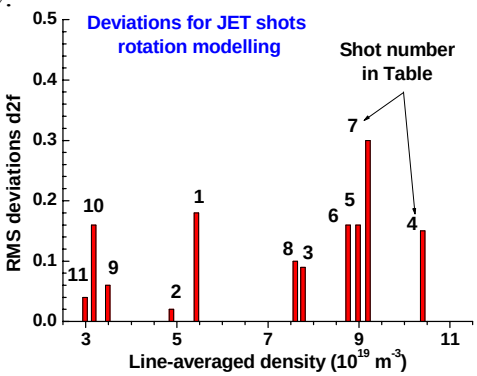

FIG. 7. RMS deviations of angular frequency for 11 JET shots of Table 1

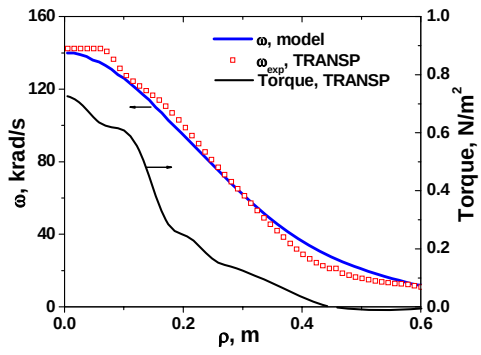

FIG. 8. The profiles of deposited torque, calculated angular rotation frequency ω and experimental one ω_{exp} for MAST shot #18696.

Figure 7 shows RMS deviations of angular frequency $d_2\omega$ averaged over the time intervals Δt ~ 1-2 s for shots with currents $I_p > 1.5$ MA, and ranked with plasma density. We see that the deviations are generally less than 10-15%.

The developed model was applied to MAST experiment. For this device the coefficient C_ω in (37), found from the analysis of 3 shots, is smaller: $C_\omega = 0.5 / n^{1/3}$. Figure 8 shows the profiles of deposited torque (from TRANSP), calculated angular rotation frequency ω and the experimental one, ω_{exp}, for the shot #18696. It is seen that for MAST the calculated and experimental profiles are also close one to another.

Conclusions

The variational problem of the minimising plasma energy allowed us to find the canonical profile of the toroidal rotation angular velocity. The transport model based on this canonical profile has been calibrated to describe reasonably the velocity of forced toroidal rotation of JET plasmas. The RMS deviations of calculated rotation profiles from the experimental ones do not exceed 10-15%.

Acknowledgements

This work was partly carried out within the framework of the European Fusion Development Agreement Work, and partly funded by the UK EPSRC under grant EP/G003955 and the EC under the contract of Association between EURATOM and CCFE, and by RFBR Grant 08-07-00182. The views and opinions expressed herein do not necessarily reflect those of the European Commission.

References

[1] de VRIES, P.C., et al., Nucl. Fusion **46** (2006) 065006.
[2] BATEMAN, G., et al., 22-nd IAEA Fusion Energy Conference, FEC-2008, "Integrated modeling simulations of toroidal momentum transport in tokamaks", Paper TH/P8-35.
[3] HSU, J.Y., Chu, M.S., Phys. Fluids **30** (1987) 1221.
[4] KADOMTSEV, B.B. Sov. J. Plasma Phys. **13** (1987) 443.
[5] DNESTROVSKIJ, Yu.N. et al., Plasma Phys. Rep. **28 (**2002) 887.
[6] DNESTROVSKIJ, Yu.N., DNESTROVSKIJ, A.Yu. and LYSENKO, S.E., Plasma Phys. Rep. **31 (**2005) 529.
[7] DNESTROVSKIJ, Yu.N., et al., Plasma Phys. Control. Fusion **49 (**2007)1477.
[8] DNESTROVSKIJ, Yu.N., et al., 22-nd IAEA Fusion Energy Conference, FEC-2008, Rep. TH-P8-23.
[9] DNESTROVSKIJ, Yu.N., et al., Nucl. Fusion **31 (**1991) 1877.
[10] DNESTROVSKIJ, Yu.N., et al., Plasma Phys. Rep. **36** (2010) 645.
[11] DNESTROVSKIJ, Yu.N., et al., Nucl. Fusion **35** (1995) 1047.
[12] POLITZER, P.A., et al., Nucl. Fusion **48** (2008) 075001.
[13] MANTICA, P., et al., Phys. Rev. Lett. **102** (2009) 175002.
[14] ROACH, C.M., et al., Nucl. Fusion **48** (2008) 125001.
[15] TALA, T., et al., Phys. Rev. Lett. **102** (2009) 075001.